Original Article

670 nm photobiomodulation improves the mitochondrial redox state of diabetic wounds

Shima Mehrvar[1#], Soudeh Mostaghimi[1#], Farnaz H. Foomani[1], Betsy Abroe[2], Janis T. Eells[3], Sandeep Gopalakrishnan[2], Mahsa Ranji[1]

[1]Biophotonics Lab, Department of Electrical Engineering, [2]College of Nursing, [3]Department of Biomedical Sciences, University of Wisconsin Milwaukee, Milwaukee, WI, USA

[#]These authors contributed equally to this work.

Correspondence to: Mahsa Ranji. 3200 N Cramer St, Eng & Math Sciences 1195, Milwaukee, WI 53211, USA. Email: ranji@uwm.edu; Sandeep Gopalakrishnan. 1921 E Hartford Ave, Cunningham Hall 455, Milwaukee, WI 53211, USA. Email: sandeep@uwm.edu.

Background: Photobiomodulation (PBM) by far-red (FR) to near-infrared (NIR) light has been demonstrated to accelerate diabetic wound healing in preclinical and clinical studies. Mitochondrial dysfunction and oxidative stress play key roles in impaired diabetic wound healing, and the effect of PBM on the metabolic state of diabetic wounds remains to be elucidated.

Methods: In this study, a custom-designed *in vivo* fluorescence imaging technique was used to quantitatively assess the effect of FR-PBM on the mitochondrial bioenergetics of diabetic wounds. The intrinsic fluorescence of two mitochondrial co-enzymes, nicotinamide adenine dinucleotide (NADH) and oxidized flavin adenine dinucleotide (FAD), was monitored to quantify the redox ratio (RR) (NADH/FAD) of wounds over time.

Results: Using an excisional model of wound healing, we demonstrated that 670 nm (FR) PBM improved mitochondrial bioenergetics and stimulated the rate of wound healing in diabetic *db/db* mice. Wound closure and the RR of diabetic wounds in response to 670 nm PBM (4.5 J/cm^2, 60 mW/cm^2 for 90 s per day, 5 days/week) were compared to the sham-treated group. At day 9 of post-wounding, we observed a 43% decrease in the wound area and a 75% increase in RR in FR-treated diabetic mice compared to sham-treated diabetic mice.

Conclusions: We conclude that the increase in mitochondrial RR and the related decrease in oxidative stress may be an important factor in FR-PBM mediated acceleration of wound healing in diabetic mice.

Keywords: Redox state; photobiomodulation (PBM); diabetic wounds; nicotinamide adenine dinucleotide (NADH); flavin adenine dinucleotide (FAD)

Submitted Apr 02, 2020. Accepted for publication Jul 10, 2020.
doi: 10.21037/qims-20-522
View this article at: http://dx.doi.org/10.21037/qims-20-522

Introduction

Wound healing is a complex and dynamic biological process that involves overlapping phases of hemostasis, inflammation, proliferation, and remodeling (1). Excessive and uncontrolled oxidative stress has been shown to contribute to a perpetual inflammatory state, deregulate the healing process; thus, playing a central role in the pathogenesis of chronic non-healing wounds (2,3). Chronic non-healing wounds are generally believed to develop when the acute inflammatory phase of wound healing progresses to chronic inflammation without resolution (4). Chronic lower-extremity ulcers are a common complication of diabetes, and approximately 15% to 25% of individuals diagnosed with diabetes will develop lower extremity ulcers or foot ulcers at some point in their lifetime (5). Moreover, diabetic ulcers often persist for months to years in

debilitated patients (6-8). These ulcers can become infected, causing pain, discomfort, hospitalizations, and poor quality of life, which impose a tremendous economic burden on the healthcare system with costs conservatively estimated for the management of diabetic foot ulcers to be $9–13 billion in the United States (9). This gives rise to a secondary demand; a need to be able to monitor and track the cellular changes during the wound healing trajectory, so that effective interventions can be identified and implemented during the early stages benefiting the patient population (2).

Current treatment strategies for wound management in diabetic patients involve debridement, topical antibiotics, the application of topical dressings, and oftentimes surgery (10). Clinical Studies have shown that interventions like hyperbaric oxygen therapy (HBOT) and extracorporeal shock wave therapy can improve the process of diabetic wound healing (11-15). Photobiomodulation (PBM) using far-red (FR) to near-infrared (NIR) light is a non-invasive, painless, and inexpensive therapeutic modality with documented efficacy in preclinical and clinical studies in soft-tissue injuries and wound healing (16,17). FR/NIR photons interact with the mitochondrial photo-acceptor molecule, cytochrome c oxidase (CcO), the terminal electron acceptor of the electron transport chain (ETC) (18,19). This interaction modifies nicotinamide adenine dinucleotide (NADH) linked dehydrogenase reactions (20) and alters the rate of ADP/ATP exchange (21), resulting in improved mitochondrial bioenergetics and activating intracellular signaling pathways that decrease chronic inflammation and promote healing (22). Studies have shown that different wavelengths from red to FR and NIR have different effects on ATP synthesis. It has been observed that light irradiation at wavelengths of 477 and 554 nm did not affect the ATP synthesis, while 415, 602, 632.8, 650, and 725 nm could enhance it (23). The irradiation duration and the amount of power density (irradiance) can also alter the results and, in some cases, inverse the effect and increase the inflammation (24). Many of the cellular and mechanistic events of PBM that promote wound healing is poorly understood. The objective of this study was to non-invasively assess the effect of 670 nm PBM on metabolic activity and oxidative stress in diabetic wounds.

In the mitochondrial ETC, two primary electron donors are the NADH and FADH2 (flavin adenine dinucleotide) (25,26). NADH and FAD (the oxidized form of FADH2) are mitochondrial metabolic co-enzymes, which are auto-fluorescent. Imaging NADH and FAD is one of the methods vastly used to study mitochondria bioenergetics. Fluorescence spectroscopy (27), fluorescence lifetime imaging (28) and two-photon fluorescence imaging (29) are the most common *in vivo* fluorescence imaging technologies used. We have previously shown that our custom-designed *in vivo* fluorescence imager can successfully be used as an optical indicator of the complex wound healing process in diabetes (30). The fluorescent signals of these two fluorophores have been used as an indicator of tissue metabolism in multiple animal injury models (31-33).

Our fluorescence imager enables us to capture the real-time metabolic images (NADH and FAD) of the wounds *in vivo*. The redox ratio (RR) (NADH/FAD) serves as a quantitative indicator of the mitochondrial redox state (31,32). In the current study, the fluorescence imager is utilized to test the hypothesis that PBM would accelerate the healing process in the db/db mice model of diabetes by affecting the mitochondrial redox state. We have also investigated the wound healing process in diabetic mice on biopsy samples using optical cryo-imaging. Fluorescence cryo-imaging provides a 3D volumetric redox state of tissue at the cryogenic temperature (31-33).

Methods

Experimental protocols

Animals

Genetically diabetic mice (*db/db*$^{-/-}$ mice; BKS.Cg-Dock7m +/+ Leprdb/J), 8 weeks of age were obtained from Jackson Laboratories (Bar Harbor, ME) and used in this study. *db/db*$^{-/-}$ mice is a well-characterized and widely used rodent model of type 2 diabetes and diabetic wound healing (34,35). The mice were littermates and housed under conditions of controlled temperature and illumination in an animal care facility with a 12-hour light/dark cycle throughout the acclimation and test periods. Hyperglycemia in the *db/db* mice was confirmed by regular blood glucose monitoring from tail snips using a glucometer.

FR treatment protocol

Light treatment was performed using 670 nm LED arrays engineered to eliminate heat [670±10 nm GaAlAs LED arrays (75 cm^2), Quantum Devices, Barneveld, WI]. Diabetic db/db mice were randomly assigned to 670 nm PBM or sham treatment groups. Treatment consisted of positioning the 670 nm LED array 1–2 cm directly above the wound surface and irradiating the wound for 90 seconds at an irradiance of 60 mW/cm^2 once per day for five days

per week to deliver a dose (radiant exposure) of 4.5 J/cm^2 at the wound surface for each treatment. The dosage and wavelength of irradiation are chosen based on their documented efficacy in preclinical and clinical studies for superficial treatments (36,37). Sham-treated mice had the LED array positioned above the wound for 90 seconds, but the LED array was turned off.

Excision wound model

General anesthesia was induced using 4% isoflurane in 100% oxygen (flow rate 1 L/min), and the anesthesia was maintained using 1–3% isoflurane during the surgery. All animals received 5 mg/kg carprofen SC before the surgery. The operative region was prepared by removing fur with clippers from the base of the neck to 3 cm further down the back and between the two shoulder blades. The skin was wiped with 10% povidone-iodine (Betadine) followed by Isopropyl Alcohol (74% w/w) three times before draping the mouse. A disposable sterile 4 mm biopsy punch was used to outline two circular patterns for the wound on either side of the mouse's midline at the level of the shoulders. The skin was lifted in the middle of the outline using serrated forceps. Then, a full-thickness wound was created using iris scissors. The wound was extended through the subcutaneous tissue, and the circular piece of tissue was excised. After the surgery, animals were individually caged and maintained on delta phase isothermal pads (Braintree Scientific, Inc.) until fully recovered. All animals undergoing the wound excision received 5 mg/kg carprofen SC at 24- and 48-hour post-surgery and were monitored twice daily for 3 days for manifestations of pain and once a week for weight loss.

Time-line and tissue preparation

A total of 16 diabetic mice were utilized in this investigation, all of which went through the wound induction surgery. Five of them were sacrificed immediately after biopsies for cryo-imaging at day 0 were collected. The harvested wound samples were flash frozen. *In vivo* fluorescence imaging was performed at days 0, 3, 6, and 9 post-wounding on the remaining group of mice (n=6 FR-PBM, n=5 sham-treated). The imaging of wounds was performed after the wounds on mice finished receiving the treatment. Therefore, there will be no interference of PBM in the imaging procedure, and the NADH and FAD excitation/emission will not interfere with the effect of 670 PBM on the wound healing process. The imaging procedure takes around 5 min, and during this time, all the animals are kept anesthetized, which minimizes movement artifacts during imaging. At the end of the experimental protocol, at day 9 of post wounding, the entire wounds were excised and snapped frozen immediately. The frozen biopsies were then imaged by cryo-imaging for the volumetric redox study.

In vivo fluorescence imager

Instrument

A complete description of the implementation and the design of the fluorescence imaging system can be found in our previous study (30). In short, an XYZ translational micro-positioner (ThorLabs, NJ) is used to control the field of view on XY direction. The Z-direction of the positioner movement controls the working distance and the focus of the images. The fiber-guiding light from a mercury arc lamp (Intensilight, Nikon, Tokyo, Japan) passes through optical filters to specifically excite autofluorescence (NADH and FAD) from the surface of the wounds. The emitted light from the wound passes through another set of optical filers. The excitation filter for NADH was set at 350 nm (80-nm bandwidth). The FAD excitation filter was set at 437 nm (20-nm bandwidth). NADH and FAD emission filters were set at 460 nm (50-nm bandwidth) and 537 nm (50-nm bandwidth), respectively. Two neutral density filters (ThorLabs, NJ) were used as excitation and emission filters for white light channel imaging. For selective control of imaging channels (NADH, FAD, or white light), two motorized filter wheels were used, one for excitation and one for emission. The emitted light was captured by a charge-coupled device (CCD) camera (QImaging, Rolera EMC2).

Linearity test of *in vivo* fluorescence imager

This test is performed to assess the linearity response of the system. Cuvettes containing dilution of NADH and FAD fluorescent dyes (Sigma-Aldrich Inc., St. Louis) were imaged. The concentrations were chosen based on tissues' physiological relevant range (38). The mean ± standard deviation (SD) of the images is calculated, and linear regression is performed (*Figure 1*). For correlations between measurements, a Pearson correlation coefficient was determined. *Figure 1A* shows that the NADH channel of fluorescence imager is linear with the changes in the concentration of NADH (R^2=0.98, P<0.001), while in *Figure 1B*, the intensity of the captured NADH images remained constant with FAD concentration variations. These results suggest that the NADH channel is sensitive to NADH solely, and it is unresponsive to FAD concentration

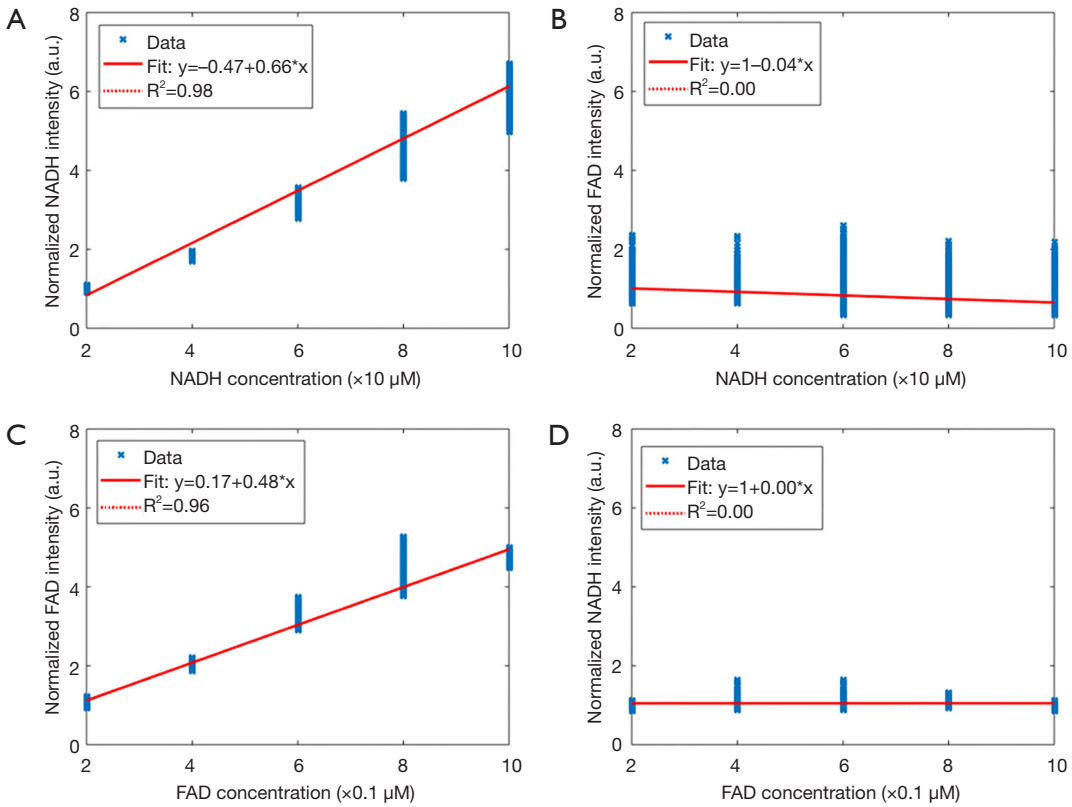

Figure 1 The results of the linearity test for the fluorescence imager using exogenous NADH and FAD solutions: the NADH (A) and FAD (B) response of the system to the increase in NADH concentrations. The NADH (C) and FAD (D) response of the system to the increase in FAD concentrations. The fitted linear regression is shown as a line, and the R2 values are included in the legends. The *in vivo* fluorescence imager used in our study is linear in the biologically relevant concentrations of NADH and FAD, and there is no cross-relation between the two channels. NADH, nicotinamide adenine dinucleotide; FAD, flavin adenine dinucleotide.

variations. Similarly, by increasing the concentration of FAD in the solutions, the intensity of captured FAD images increases linearly (*Figure 1C*, R^2=0.98, P<0.001), and the intensity of NADH images remained constant (*Figure 1D*). Therefore, the fluorescence imager used in our study is linear in the biologically relevant concentrations of NADH and FAD, and there is no cross-relation between the two channels. Furthermore, it can be inferred that the intensities of the cryo-images correlated linearly with the amount of the autofluorescence signal from the samples.

Image processing

The image processing algorithm was written in MATLAB and described in our previous publication (30). Briefly, white light images were used to segment the wounded area from the background skin manually. The same mask will be used to segment the wound from the background skin in NADH and FAD channel. The reason is that the white light images would provide us with more precise information about the area of the wound based on intensity. The method that we used is very similar to the manual methods that clinicians use to trace the wound boundaries with clear acetate (39). To minimize the day to day variation of the light source, the images were calibrated with a factor derived from an image of a cuvette containing a solution of 50 μM NADH and 0.5 μM FAD. Then, the ratio of the autofluorescence images (RR = NADH/FAD) was calculated pixel by pixel. The mean of RR histograms was considered as the quantitative marker, called Surface RR.

The RR change rate is the difference between the mean RR of samples in two consecutive data collection days. This biomarker is used to evaluate the temporal differences in the *in vivo* RR changes at different days. The negative value of the RR change rate corresponds to a descending trend in

the RR, i.e., a drop in the RR by a decrease in mitochondrial redox state and an increase in oxidative stress.

The wound area can be approximated by the number of wound pixels multiplied by pixel size. Knowing that the pixel size in the images is 40 μm × 40 μm, we can use the following equation for calculating the normalized wound area at day t:

$$Normalized\ Wound\ Area = \frac{PS(t)\times N(t)}{PS(0)\times N(0)} = \frac{N(t)}{N(0)} \quad [1]$$

where $N(t)$ is the number of wound pixels at day t. $N(0)$ is the number of wound pixels at day 0, i.e., the initial wound area. $PS(t)$ is the pixel size at day t, and $PS(0)$ is pixel size at day 0. Since the pixel size remained unchanged, we can remove it from the denominator and nominator. This simplifies the equation in a way that we can say the normalized wound area is equal to the number of pixels at day t to the number of pixels at day zero.

The wound closure rate was defined as the difference in wound area over two consecutive data collection days and was used to determine the rate of wound healing. The closure rate provides a quantitative index of wound healing over time. A positive value in the closure rate corresponds to a decrease in the wound area, and the negative value of the closure rate corresponds to an increase in the wound area.

Three-dimensional (3D) fluorescent cryo-imager

3D fluorescent cryo-imager was custom-designed at Biophotonics Lab, University of Wisconsin Milwaukee. This instrument has been described in detail in our previous studies (31-33). This device captures the metabolic state of the tissue at the cryogenic temperature. The system has a mercury arc lamp as the excitation light source (200 W lamp, Oriel, Irvine, CA, in the light source from Ushio Inc., Japan). The light passes through a filter wheel, which has NADH (350 nm with 80 nm bandwidth) and FAD (437 nm with 20 nm bandwidth) optical filters. The light is air-guided toward the sample, and emitted light passes through the emission filter wheel, which contains the specific emission filters for NADH (460 nm with 50 nm bandwidth) and FAD (537 nm with 50 nm bandwidth). Then, the image will be acquired using a CCD camera (QImaging, Aqua). A microtome blade cuts through the sample with a specified thickness (30 μm for this study), and the images are captured sequentially.

The cryo-images were processed using MATLAB. NADH and FAD images were calibrated with images captured from a flat field for NADH and FAD channels, respectively. The background (low-intensity) voxels were set to zero, and 3D redox images were obtained by calculating the RR for each voxel. The mean of RR histograms was considered as the quantitative marker, called Volumetric RR.

Statistical analysis

All the statistical analysis was conducted using SPSS. The Surface RR, Volumetric RR, and Normalized wound area in both groups of mice (sham-treated and FR-PBM) were assessed using two-factor repeated ANOVAs. Tukey's *post hoc* analysis was used with the significant criteria $P<0.05$.

Results

In vivo fluorescence imaging of wound healing

Figure 2 shows the bright-field images of representative wounds over time. The sham-treated wound showed no visual indications of healing from day 0 to day 9. In contrast, the FR-treated wound shows a conspicuous reduction in the wound area from day 0 to day 9. Representative fluorescent images of FR-treated and sham-treated wounds from days 0, 3, 6, and 9 are shown in *Figure 3*. The data in *Figure 3* at days 6 and 9 show that the RR in the FR-treated wounds is greater than the RR measured in sham-treated mice. This reflects a decrease in NADH and an increase in the FAD concentrations of the FR-treated wounds over time, resulting in a visibly greater RR at days 6 and 9.

Figure 4 depicts the histograms of *in vivo* images over time and quantifies the temporal data shown in *Figure 3*. The percentage difference between the mean value of histograms (Surface RR) from sham-treated *vs.* FR-PBM is shown for each day of post-wounding (n=5 sham-treated, n=6 FR-PBM). As it can be seen in *Figure 4*, at days 0 and 3 of post-wounding, the histograms of the *in vivo* images were not significantly different in sham-treated and FR-PBM groups. However, the difference becomes significant at days 6 and 9.

Table 1 presents the data and the statistical analysis for FR-PBM and sham-treated groups of mice over the time course of the experiment. As previously described in methods, Surface RR and wound area were obtained using *in vivo* fluorescence imager, and their corresponding changes over time are the RR change rate and closure rate, respectively. FR-treatment resulted in a significant increase

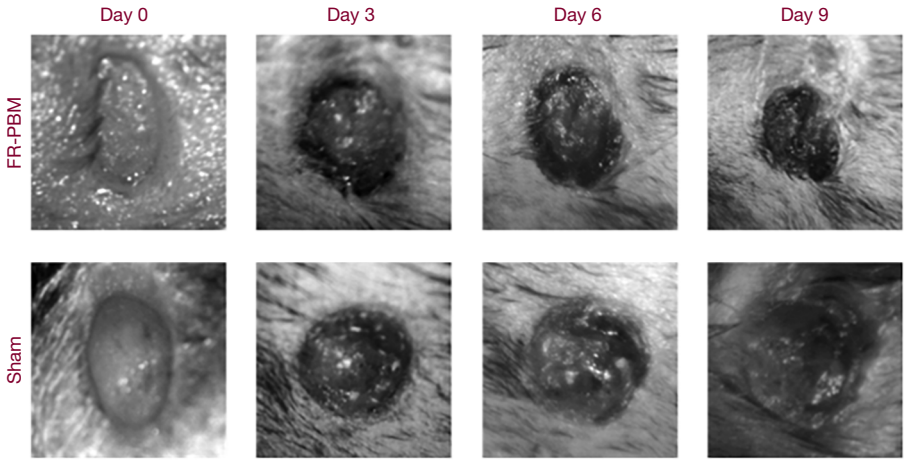

Figure 2 Representative bright-field images of the wounds over time.

in Surface RR at days 6 and 9, and the change rate of surface RR became significant at day 9. Thus, over the time course of the experiment, the mitochondrial redox state of the wounds in the FR-PBM group increased at a faster rate than the sham-treated group.

In sham-treated diabetic mice, normalized wound area increased from day 0 to day 3 and resulted in a negative rate of wound closure, i.e., the area of the wounds at day 3 was greater than that at day 0). Despite the gradual decrease in the wound area from day 3 to day 9 in sham-treated mice, the wound area at day 9 was still greater than the wound area at day 0. In contrast, wounds treated with FR light (FR-PBM group) showed evidence of healing reflected in a decrease in wound area from day 0 to day 9. The normalized wound area in the FR-PBM and sham-treated groups were significantly different on days 3, 6, and 9. By day 9, the mean wound area in the FR-PBM group was 44% smaller than the mean wound area in the sham-treated group.

3D cryo-imaging of wound healing

Figure 5A shows representative 3D rendered cryo-images captured from the biopsies collected at the beginning and the end of the experimental protocol. The color-coded images of wound biopsies show higher NADH and lower FAD in the FR-PBM group in comparison with the sham-treated group, resulting in a higher volumetric RR. *Figure 5B* illustrates the histograms of the corresponding RR images, as shown in *Figure 5A*. The histogram of sham-treated wounds at day 9 has shifted to the left when compared to the day 0 wound histogram. Also, we can see that the histogram of sham-treated wounds at day 0 and FR-PBM wounds at day 9 are centered almost at the same place, but the histogram of FR-PBM is more widely distributed. The mean volumetric RR ± standard deviation in three groups of wounds is shown in *Figure 5C*. The Volumetric RR of sham-treated wounds at day 9 significantly dropped by 33% when compared to the sham-treated mice at day 0. Also, FR-PBM caused a significant 46% increase in the volumetric RR of wounds at day 9 when compared to the sham-treated wounds at day 9. This observation confirms the data that was obtained from the *in vivo* fluorescence imager. The supplementary Figures S1,S2 show 2D and 3D redox ratio images of the wound biopsies of all animals over time.

Discussion

Cellular function is significantly impaired in diabetic wound healing (40). The hypoxic wound microenvironment in diabetes resulting from poor vascularization and impaired blood flow contributes to high oxidative stress. Diabetic wound healing is further compromised by hyperglycemia, neuropathy, and dysfunctional immune cells (41). Impairment is also characterized by decreased cellular migration, proliferation, reduced NO synthesis, a reduction in growth factors, and decreased collagen synthesis. Proteinases that degrade the extracellular matrix and collagen (MMPs) are also increased in diabetic wound healing (17). Increasing evidence indicates that mitochondrial reactive oxygen species (ROS) play an

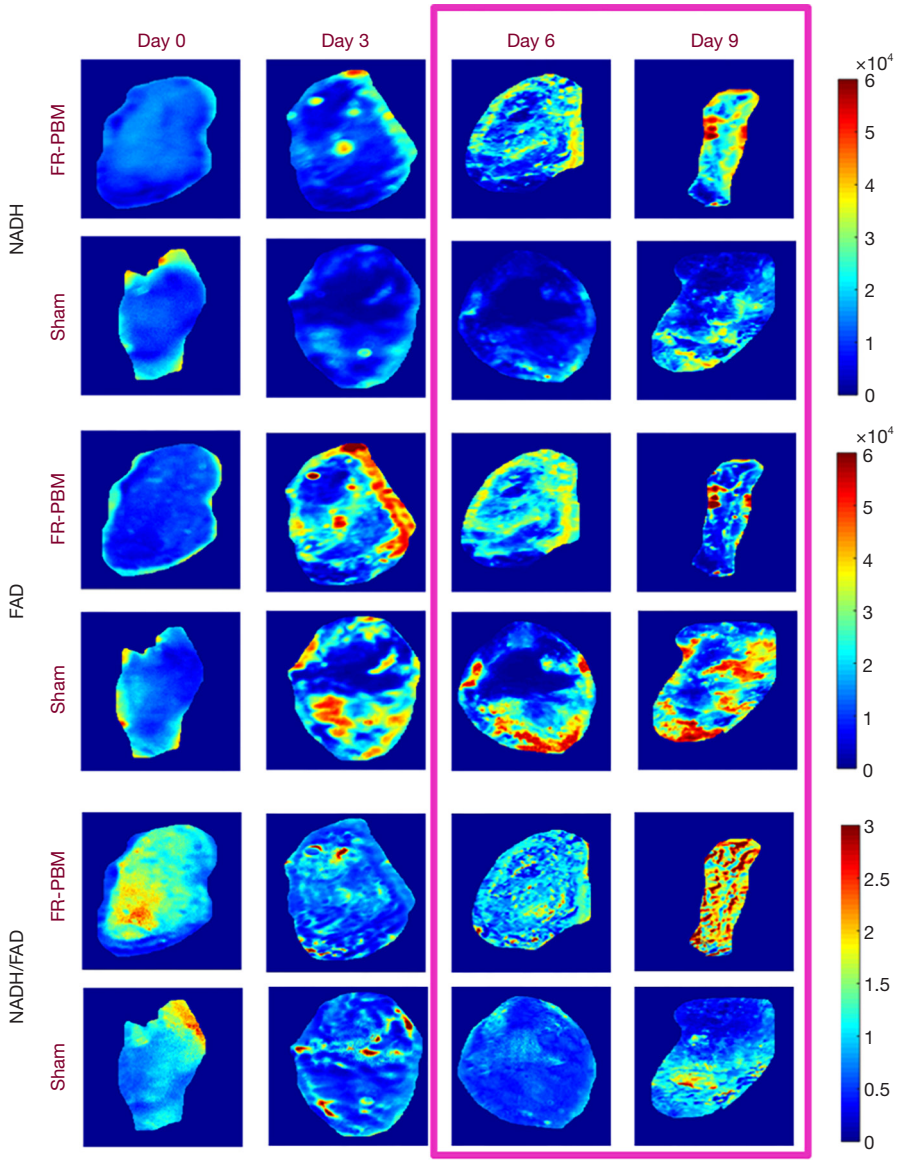

Figure 3 Representative *in vivo* fluorescence images of NADH, FAD, and the tissue redox ratio (NADH/FAD) for representative wounds over days: unlike the wound on the sham-treated mice, the FR-PBM treatment increased the NADH intensity of the wounds and decreased the FAD intensity. Therefore, at days 6 and 9 of post wounding, the wound on FR-PBM mice showed a higher redox ratio in comparison with sham-treated mice. NADH, nicotinamide adenine dinucleotide; FAD, flavin adenine dinucleotide; FR, far-red; PBM, photobiomodulation.

important role in the delayed wound healing in diabetes, and mitochondria-targeted antioxidant strategies have been shown to improve healing (3,42). PBM by FR/NIR light has been shown to improve diabetic wound healing (17,43-47). Studies have documented that PBM improved mitochondrial bioenergetics (44), increased transforming growth factor-1 (46), increased collagen production, cell migration, and proliferation (45-47). In addition, pro-inflammatory cytokines and MMPs are down-regulated by PBM (43).

The intracellular chromophore hypothesized to be the central player in the molecular mechanism of PBM is CcO, the terminal enzyme of the ETC. CcO plays a central role in cellular bioenergetics and regulates

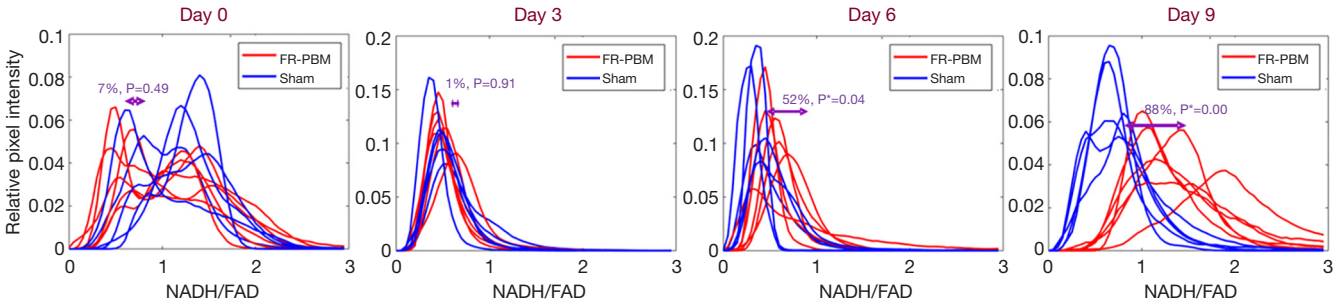

Figure 4 The redox ratio the histogram of the wounds on the FR-PBM and the sham-treated group of mice at each day of the experimental protocol: unlike the wound on the sham-treated mice, the FR-PBM showed a right shift in their redox ratio histograms. Therefore, as time passed, the wound on FR-PBM mice showed a higher mean redox ratio. FR, far-red; PBM, photobiomodulation.

Table 1 Quantitative assessment of FR-PBM (*in vivo*): the surface RR, RR change rate, normalized wound area, and closure rate are calculated by *in vivo* fluorescence imager

Variables	Group	Day 0	Day 3	Day 6	Day 9
Surface RR	FR-PBM	1.01±0.07	0.46±0.03	0.55±0.05*	1.26±0.07*
	Sham	1.08±0.07	0.47±0.05	0.36±0.06	0.67±0.04
RR change rate	FR-PBM	–	–0.54±0.07	0.09±0.05	0.71±0.08*
	Sham	–	–0.61±0.11	–0.05±0.06	0.25±0.04
Normalized wound area	FR-PBM	1	0.87±0.08*	0.82±0.02*	0.61±0.09*
	Sham	1	1.32±0.14	1.26±0.09	1.08±0.11
Closure rate	FR-PBM	–	0.13±0.08*	0.05±0.06	0.21±0.11
	Sham	–	–0.32±0.14	0.06±0.10	0.18±0.11

The values are mean ± standard deviation, and stars (*) mark the values in the FR-PBM group that are significantly different from the sham-treated group with the criteria of P<0.05. FR, far-red; PBM, photobiomodulation; RR, redox ratio.

secondary cell signaling pathways involved in the activation of transcription factors, leading to altered gene transcription and enhanced protein synthesis of antioxidants, cytokines, and growth factors thus creating a stable microenvironment for cell proliferation, migration, and survival. Karu (48) proposed mitochondrial retrograde signaling in NIR PBM and demonstrated that the effects are mediated via mitochondrial membrane potential ($\Delta\Psi m$), generation of ROS, altering the (Ca^{2+}) dynamics in the cell, and influencing photodissociation of NO from CcO. The epidermal chromophores are varied based on their location, distribution, and structure (49). Some of which that are potentially targeted by FR/NIR PBM are melanin, nitrosylated hemoglobin and myoglobin. It has been shown that FR light photodissociates NO, resulting in vasodilation, thus increasing the trafficking of immune cells promoting wound healing (50).

The endogenous fluorescent co-enzymes, reduced NADH and FAD, play a pivotal role in cellular metabolism. The quantitative assessment of their presence in living cells can be exploited to monitor cellular energetics (51). By imaging mitochondrial co-enzymes, NADH and FAD, it is possible to probe the mitochondrial redox state of the diabetic wounds and wound healing status over time. We have previously shown that NADH and FAD can be optically monitored during wound healing, and the ratio of these two, RR, can be used as the indicator of tissue metabolism during wound healing (30). However, to the best of our knowledge, there has been no other study that has examined the effect of FR-PBM on the mitochondrial redox state during diabetic wound healing.

Consistent with our previous report (30), we have seen a reduction in the mitochondrial redox state of wounds in a spontaneous diabetic model of type 2 diabetes, *db/db*$^{-/-}$ mice

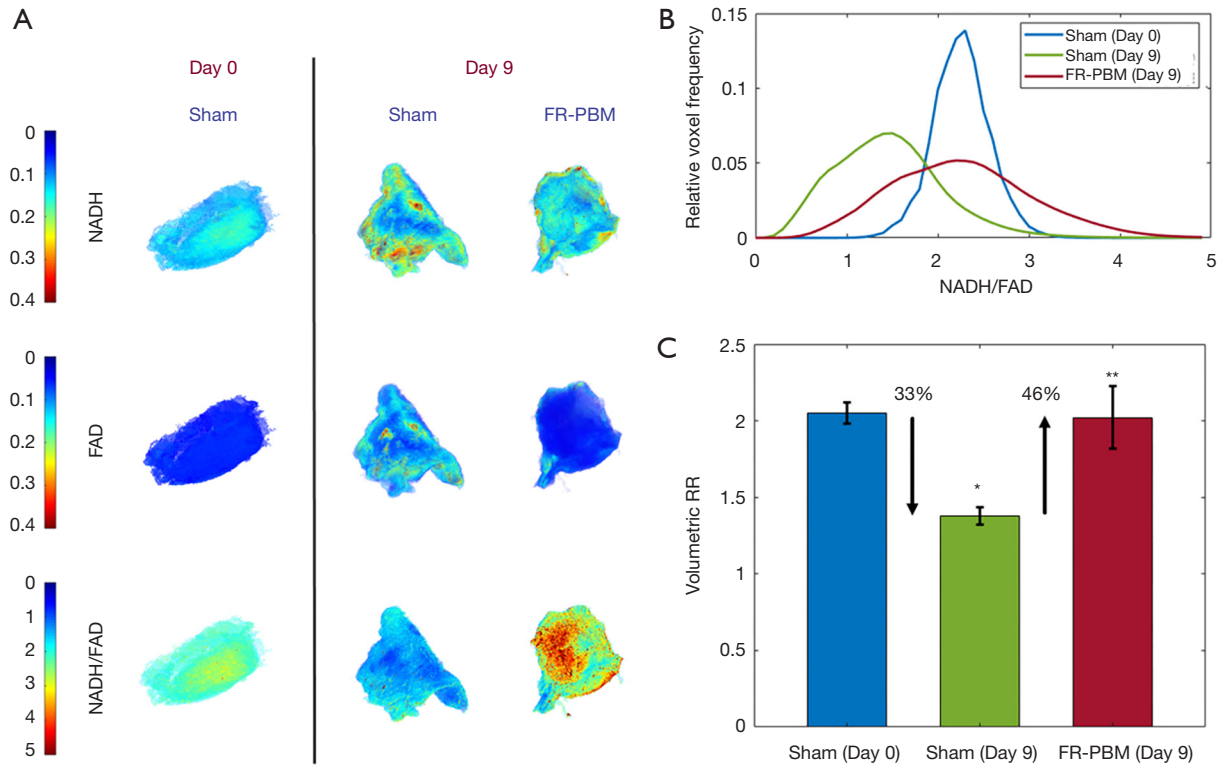

Figure 5 The cryo-imaging results of sham-treated *vs.* FR-PBM treated wounds. (A) Representative fluorescence cryo-images of NADH, FAD, and the tissue redox ratio (NADH/FAD) for representative wounds are shown at days 0 and 9. (B) The redox ratio histogram of the wounds on the FR-PBM and sham-treated mice. (C) The volumetric redox ratio ± standard deviation of representative wounds in bar plots. The wound on FR-treated mice showed a 46% higher redox ratio in comparison with sham-treated controls at day 9 [n=5 sham-treated (day 0), n=5 sham-treated (day 9), and n=6 FR-PBM (day 9)]. *, significant difference between day 0 and day 9 in redox ratio of sham-treated wounds. **, significant difference between redox ratio of FR-PBM treated *vs.* sham treated wounds at day 9 of post wounding. NADH, nicotinamide adenine dinucleotide; FAD, flavin adenine dinucleotide; FR, far-red; PBM, photobiomodulation.

after nine days post wounding compared to sham-treated animals. This suggests an increase in ROS production and mitochondrial dysfunction due to the accumulation of oxidized forms (NAD and FAD) of the mitochondrial co-enzymes NADH and FADH2. The increase in ROS production contributes to progressive inflammatory response, which is highly sensitive to impairment in wound healing (52). However, PBM by FR to NIR light has been shown to help the corrupted wound healing process by restoring the function of damaged mitochondria. FR/NIR photons are absorbed by the mitochondrial photo-acceptor molecule, CcO, triggering intracellular signaling pathways that culminate in improved mitochondrial energy metabolism, increased cytoprotective factor production, and cell survival.

FR/NIR PBM improves healing outcomes demonstrated by increasing fibroblast proliferation, synthesis of collagen and procollagen, angiogenesis, and upregulating macrophage and lymphocyte function (53,54).

In this study, our custom-designed non-contact noninvasive fluorescence imager detects the wound healing trajectory after FR irradiation by monitoring the online mitochondrial metabolic state quantitatively. At days 6 and 9 of post-wounding, the RR (NADH/FAD) of FR-treated wounds in diabetic mice was higher than those of sham-treated animals. The cryo-imaging studies confirmed the results from *in vivo* fluorescence imaging. The histograms from cryo-images of FR-treated animals at day 9 of post-wounding showed similar results to sham-treated animals at day 0, almost the same surface RR but with a wider distribution in the intensity of NADH/FAD. This wider distribution of RR shows the heterogeneity in the RR of

healing wounds compared to day 0 wounds.

The results from both *in vivo* fluorescence imager and cryo-imager showed that the treatment with 670 nm FR photons accelerated the wound healing by increasing the RR significantly, indicative of protection of mitochondrial function, and a reduction of oxidative stress. These results support previous investigations documenting the ability of FR-PBM in decreasing oxidative stress and improving mitochondrial function (55,56). Our findings strongly support our hypothesis that diabetes-induced mitochondrial dysfunction is mitigated by FR PBM, resulting in accelerated wound healing. The development and application of this effective photoceutical wound healing treatment will improve our ability to deal with the high prevalence of foot ulcers in the diabetic population. Moreover, the instrumentation developed by our research team facilitates analysis of the metabolic status of the wound over the time course of wound healing and enable monitoring of the wound healing trajectory. We aim at implementing a microscopic cryo-imager in the near future with a cellular resolution that would allow us to study the effect of PBM-light treatment on the RR of various types of cells in the wound.

Acknowledgments

Funding: This research was funded by Office of Research, University of Wisconsin Milwaukee under grants RACAS #AAB1551 and RGI 101x371. This work is also partially supported by NIH R15EY031533 to MR.

Footnote

Conflicts of Interest: All authors have completed the ICMJE uniform disclosure form (available at http://dx.doi.org/10.21037/qims-20-522). The authors have no conflicts of interest to declare.

Ethical Statement: The study was approved by the Institutional Animal Care and Use Committee (IACUC, Protocol #16-17#12) at the University of Wisconsin Milwaukee, and experiments were conducted following the National Institute of Health Guide for the Care and Use of Laboratory Animals.

References

1. Li J, Chen J, Kirsner R. Pathophysiology of acute wound healing. Clin Dermatol 2007;25:9-18.
2. Enoch S, Leaper DJ. Basic science of wound healing. Surgery 2008;26:31-7.
3. Cano Sanchez M, Lancel S, Boulanger E, Neviere R. Targeting oxidative stress and mitochondrial dysfunction in the treatment of impaired wound healing: A systematic review. Antioxidants (Basel) 2018;7:98.
4. Iqbal A, Jan A, Wajid M, Tariq S. Management of chronic non-healing wounds by hirudotherapy. World J Plast Surg 2017;6:9.
5. Sen CK. Human Wounds and Its Burden: An Updated Compendium of Estimates. Adv Wound Care (New Rochelle) 2019;8:39-48.
6. Guo S, Dipietro LA. Factors affecting wound healing. J Dent Res 2010;89:219-29.
7. Fahey TJ 3rd, Sadaty A, Jones WG 2nd, Barber A, Smoller B, Shires GT. Diabetes impairs the late inflammatory response to wound healing. J Surg Res 1991;50:308-13.
8. Terranova A. The effects of diabetes mellitus on wound healing. Plast Surg Nurs 1991;11:20-5.
9. Raghav A, Khan ZA, Labala RK, Ahmad J, Noor S, Mishra BK. Financial burden of diabetic foot ulcers to world: a progressive topic to discuss always. Ther Adv Endocrinol Metab 2018;9:29-31.
10. Fernandez E, Bernhardsen B. Wound Care Management. Prim Care Rep 2018;24.
11. Löndahl M, Katzman P, Nilsson A, Hammarlund C. Hyperbaric oxygen therapy facilitates healing of chronic foot ulcers in patients with diabetes. Diabetes Care 2010;33:998-1003.
12. Duzgun AP, Satır HZ, Ozozan O, Saylam B, Kulah B, Coskun F. Effect of hyperbaric oxygen therapy on healing of diabetic foot ulcers. J Foot Ankle Surg 2008;47:515-9.
13. Kessler L, Bilbault P, ORTega F, Grasso C, Passemard R, Stephan D, Pinget M, Schneider F. Hyperbaric oxygenation accelerates the healing rate of nonischemic chronic diabetic foot ulcers: a prospective randomized study. Diabetes Care 2003;26:2378-82.

14. Wang CJ, Wu RW, Yang YJ. Treatment of diabetic foot ulcers: a comparative study of extracorporeal shockwave therapy and hyperbaric oxygen therapy. Diabetes Res Clin Pract 2011;92:187-93.
15. Greer N, Foman NA, MacDonald R, Dorrian J, Fitzgerald P, Rutks I, Wilt TJ. Advanced wound care therapies for nonhealing diabetic, venous, and arterial ulcers: a systematic review. Ann Intern Med 2013;159:532-42.
16. Jere SW, Abrahamse H, Houreld NN. The JAK/STAT signaling pathway and photobiomodulation in chronic wound healing. Cytokine Growth Factor Rev 2017;38:73-9.
17. Houreld NN. Shedding light on a new treatment for diabetic wound healing: a review on phototherapy. ScientificWorldJournal 2014. doi: 10.1155/2014/398412.
18. Ao J, Wood JP, Chidlow G, Gillies MC, Casson RJ. Retinal pigment epithelium in the pathogenesis of age-related macular degeneration and photobiomodulation as a potential therapy? Clin Exp Ophthalmol 2018;46:670-86.
19. Hamblin MR. Mechanisms and mitochondrial redox signaling in photobiomodulation. Photochem Photobiol 2018;94:199-212.
20. Passarella S, Casamassima E, Molinari S, Pastore D, Quagliariello E, Catalano IM, Cingolani A. Increase of proton electrochemical potential and ATP synthesis in rat liver mitochondria irradiated in vitro by helium-neon laser. FEBS Lett 1984;175:95-9.
21. Passarella S, Ostuni A, Atlante A, Quagliariello E. Increase in the ADP/ATP exchange in rat liver mitochondria irradiated in vitro by helium-neon laser. Biochem Biophys Res Commun 1988;156:978-86.
22. Eells JT, Henry MM, Summerfelt P, Wong-Riley MT, Buchmann EV, Kane M, Whelan NT, Whelan HT. Therapeutic photobiomodulation for methanol-induced retinal toxicity. Proc Natl Acad Sci U S A 2003;100:3439-44.
23. Karu T. Primary and secondary mechanisms of action of visible to near-IR radiation on cells. J Photochem Photobiol B 1999;49:1-17.
24. Jenkins PA, Carroll JD. How to report low-level laser therapy (LLLT)/photomedicine dose and beam parameters in clinical and laboratory studies. Photomed Laser Surg 2011;29:785-7.
25. Nuutinen EM. Subcellular origin of the surface fluorescence of reduced nicotinamide nucleotides in the isolated perfused rat heart. Basic Res Cardiol 1984;79:49-58.
26. Chance B, Schoener B, Oshino R, Itshak F, Nakase Y. Oxidation-reduction ratio studies of mitochondria in freeze-trapped samples. NADH and flavoprotein fluorescence signals. J Biol Chem 1979;254:4764-71.
27. Mokrý M, Gál P, Vidinský B, Kušnír J, Dubayová K, Mozeš Š, Sabo J. In vivo monitoring the changes of interstitial pH and FAD/NADH ratio by fluorescence spectroscopy in healing skin wounds. Photochem Photobiol 2006;82:793-7.
28. Pena AM, Boulade M, Brizion S, Tissot N, Bornschloegl T, Galey JB, Bernerd F, Planel E. editors. Multiphoton FLIM imaging of NADH and FAD to analyze cellular metabolic activity of reconstructed human skin in response to UVA light. Multiphoton Microscopy in the Biomedical Sciences XIX; 2019: International Society for Optics and Photonics.
29. Stringari C, Abdeladim L, Malkinson G, Mahou P, Solinas X, Lamarre I, Brizion S, Galey JB, Supatto W, Legouis R. Multicolor two-photon imaging of endogenous fluorophores in living tissues by wavelength mixing. Sci Rep 2017;7:3792.
30. Mehrvar S, Rymut KT, Foomani FH, Mostaghimi S, Eells JT, Ranji M, Gopalakrishnan S. Fluorescence Imaging of Mitochondrial Redox State to Assess Diabetic Wounds. IEEE J Transl Eng Health Med 2019;7:1800809.
31. la Cour MF, Mehrvar S, Kim J, Martin A, Zimmerman MA, Hong JC, Ranji M. Optical imaging for the assessment of hepatocyte metabolic state in ischemia and reperfusion injuries. Biomed Opt Express 2017;8:4419-26.
32. la Cour MF, Mehrvar S, Heisner JS, Motlagh MM, Medhora M, Ranji M, Camara AKS. Optical metabolic imaging of irradiated rat heart exposed to ischemia-reperfusion injury. J Biomed Opt 2018;23:1-9.
33. Mehrvar S, la Cour MF, Medhora M, Camara AK, Ranji M. Optical Metabolic Imaging for Assessment of Radiation-Induced Injury to Rat Kidney and Mitigation by Lisinopril. Ann Biomed Eng 2019;47:1564-74.
34. Michaels J, Churgin SS, Blechman KM, Greives MR, Aarabi S, Galiano RD, Gurtner GC. db/db mice exhibit severe wound-healing impairments compared with other murine diabetic strains in a silicone-splinted excisional wound model. Wound Repair Regen 2007;15:665-70.
35. Elliot S, Wikramanayake TC, Jozic I, Tomic-Canic M. A modeling conundrum: murine models for cutaneous wound healing. J Invest Dermatol 2018;138:736-40.
36. Hamblin MR, Demidova TN. editors. Mechanisms of low level light therapy. Mechanisms for low-light therapy; 2006: International Society for Optics and Photonics.
37. Avci P, Gupta A, Sadasivam M, Vecchio D, Pam Z, Pam N, Hamblin MR. editors. Low-level laser (light) therapy (LLLT) in skin: stimulating, healing, restoring.

Seminars in cutaneous medicine and surgery; 2013: NIH Public Access.
38. Liu Q, Grant G, Vo-Dinh T. Investigation of synchronous fluorescence method in multicomponent analysis in tissue. IEEE J Selected Topics Quantum Elect 2009;16:927-40.
39. Wendelken ME, Berg WT, Lichtenstein P, Markowitz L, Comfort C, Alvarez OM. Wounds measured from digital photographs using photo-digital planimetry software: validation and rater reliability. Wounds 2011;23:267.
40. Cianfarani F, Toietta G, Di Rocco G, Cesareo E, Zambruno G, Odorisio T. Diabetes impairs adipose tissue–derived stem cell function and efficiency in promoting wound healing. Wound Repair Regen 2013;21:545-53.
41. Kim JH, Yang B, Tedesco A, Lebig EGD, Ruegger PM, Xu K, Borneman J, Martins-Green M. High Levels of oxidative Stress and Skin Microbiome are critical for initiation and Development of chronic Wounds in Diabetic Mice. Sci Rep 2019;9:19318.
42. Demyanenko IA, Zakharova VV, Ilyinskaya OP, Vasilieva TV, Fedorov AV, Manskikh VN, Zinovkin RA, Pletjushkina OY, Chernyak BV, Skulachev VP. Mitochondria-targeted antioxidant SkQ1 improves dermal wound healing in genetically diabetic mice. Oxid Med Cell Longev 2017;2017:6408278.
43. Houreld NN, Sekhejane PR, Abrahamse H. Irradiation at 830 nm stimulates nitric oxide production and inhibits pro-inflammatory cytokines in diabetic wounded fibroblast cells. Lasers Surg Med 2010;42:494-502.
44. Zungu IL, Hawkins Evans D, Abrahamse H. Mitochondrial responses of normal and injured human skin fibroblasts following low level laser irradiation—an in vitro study. Photochem Photobiol 2009;85:987-96.
45. Ayuk SM, Houreld NN, Abrahamse H. Collagen production in diabetic wounded fibroblasts in response to low-intensity laser irradiation at 660 nm. Diabetes Technol Ther 2012;14:1110-7.
46. Pereira AN, Eduardo Cde P, Matson E, Marques MM. Effect of low-power laser irradiation on cell growth and procollagen synthesis of cultured fibroblasts. Lasers Surg Med 2002;31:263-7.
47. Frigo L, Fávero GM, Lima HJC, Maria DA, Bjordal JM, Joensen J, Iversen VV, Marcos RL, Parizzoto NA, Lopes-Martins RAB. Low-level laser irradiation (InGaAlP-660 nm) increases fibroblast cell proliferation and reduces cell death in a dose-dependent manner. Photomed Laser Surg 2010;28 Suppl 1:S151-6.
48. Karu TI. Mitochondrial signaling in mammalian cells activated by red and near-IR radiation. Photochem Photobiol 2008;84:1091-9.
49. Young AR. Chromophores in human skin. Phys Med Biol 1997;42:789.
50. Chung H, Dai T, Sharma SK, Huang YY, Carroll JD, Hamblin MR. The nuts and bolts of low-level laser (light) therapy. Ann Biomed Eng 2012;40:516-33.
51. Schaefer PM, Kalinina S, Rueck A, von Arnim CA, von Einem B. NADH autofluorescence—a marker on its way to boost bioenergetic research. Cytometry A 2019;95:34-46.
52. Brem H, Tomic-Canic M. Cellular and molecular basis of wound healing in diabetes. J Clin Invest 2007;117:1219-22.
53. Heo JC, Park JA, Kim DK, Lee JH. Photobiomodulation (660 nm) therapy reduces oxidative stress and induces BDNF expression in the hippocampus. Sci Rep 2019;9:10114.
54. Rupel K, Zupin L, Colliva A, Kamada A, Poropat A, Ottaviani G, Gobbo M, Fanfoni L, Gratton R, Santoro M. Photobiomodulation at multiple wavelengths differentially modulates oxidative stress in vitro and in vivo. Oxid Med Cell Longev 2018;2018:6510159.
55. Fitzgerald M, Bartlett CA, Payne SC, Hart NS, Rodger J, Harvey AR, Dunlop SA. Near infrared light reduces oxidative stress and preserves function in CNS tissue vulnerable to secondary degeneration following partial transection of the optic nerve. J Neurotrauma 2010;27:2107-19.
56. Eells JT, Gopalakrishnan S, Valter K. Near-infrared photobiomodulation in retinal injury and disease. Adv Exp Med Biol 2016;854:437-41.

Cite this article as: Mehrvar S, Mostaghimi S, Foomani FH, Abroe B, Eells JT, Gopalakrishnan S, Ranji M. 670 nm photobiomodulation improves the mitochondrial redox state of diabetic wounds. Quant Imaging Med Surg 2021;11(1):107-118. doi: 10.21037/qims-20-522

Supplementary

The redox ratio images of the wounds on individual mice over time are shown in *Figure S1*. *Figure S2* shows all the 3D images of the volumetric redox ratio for all the wound biopsies used in this study. The consistency in the redox ratio of the wounds on different mice (biological replicates) in the group/days signifies our research findings.

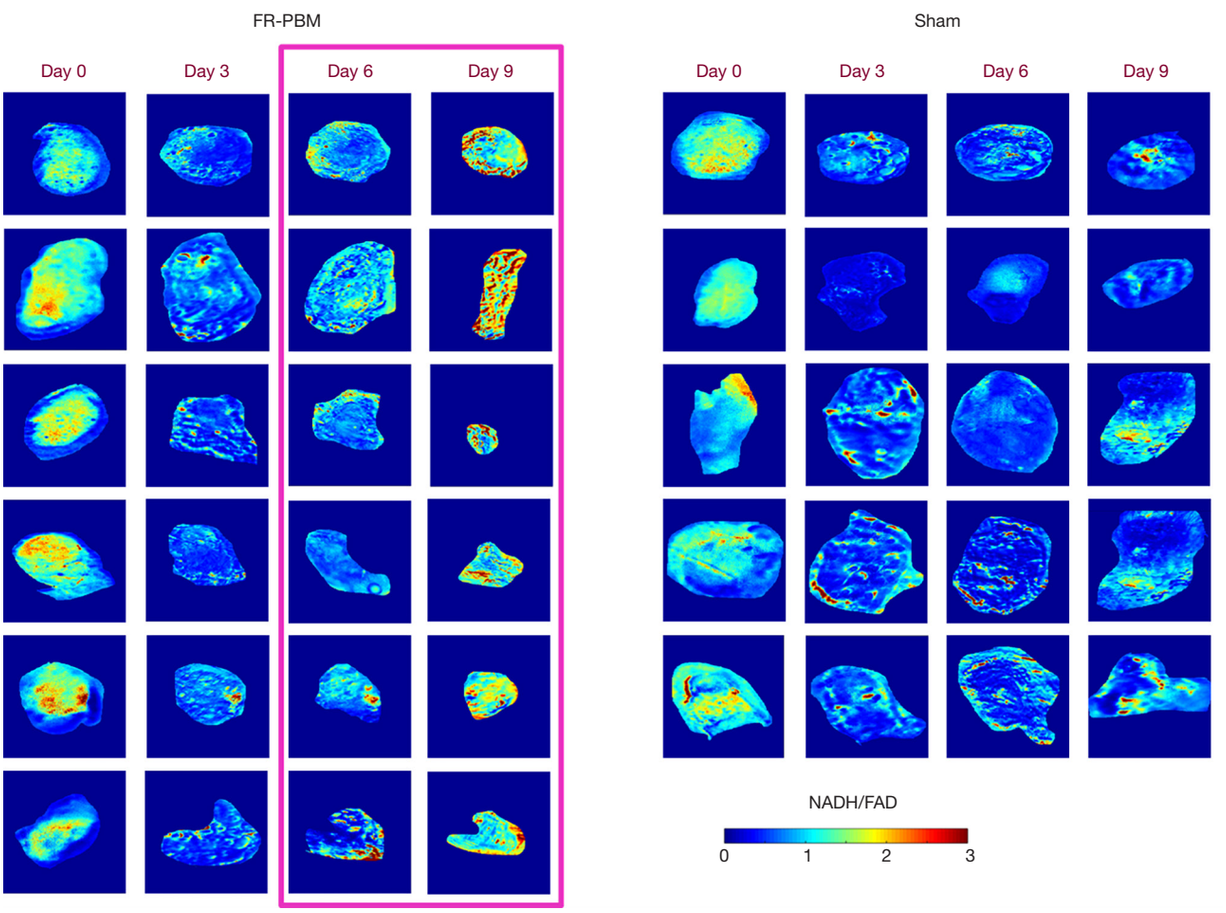

Figure S1 Surface redox ratio images of all wounds over days.

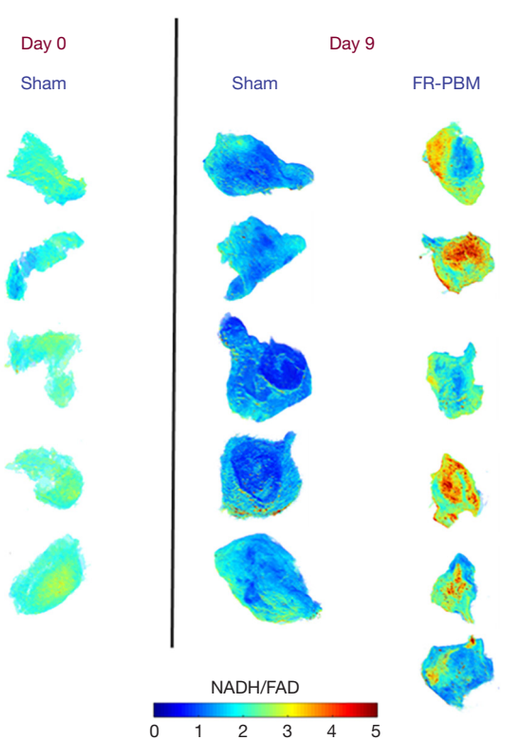

Figure S2 Volumetric redox ratio images of all wounds at days 0 and 9 of post-wounding.

http://dx.doi.org/10.21037/qims-20-522